Int J Adv Manuf Technol (2016) 86:2701–2710
DOI 10.1007/s00170-016-8373-2

ORIGINAL ARTICLE

The calculation of vertical rolling force by using angular bisector yield criterion and Pavlov principle

Jianzhao Cao[1] · **Yuanming Liu**[2] · **Fangjun Luan**[1] · **Dewen Zhao**[2]

Received: 13 September 2015 / Accepted: 13 January 2016 / Published online: 29 January 2016

Abstract The automatic width control of the strip that is used in vertical rolling is a key issue in the hot strip rolling process. It is the first time that the internal deformation power and the friction power are obtained by using angular bisector yield criterion and Pavlov projection principle in the vertical rolling. At the same time, the shear power is determined by use of the integral mean value theorem. Then the vertical rolling force and shape parameters are obtained by minimizing the total power functional. The relative error of rolling forces is less than 8.29 % compared with those measured on-line in a hot strip rolling plant. Moreover, the formula forms of the three powers mentioned above are greatly simplified and improved.

Keywords Vertical rolling · Dog-bone shape · Angular bisector yield criterion · Analytical solution

1 Introduction

Nowadays, the vertical rolling process is widely used to control width in the roughing stands of a hot strip mill. The rolling, also referred as edge rolling or slab edge, is a typical deformation problem of the super-high work piece. At this stand, deformation is mainly localized close to the rolls and gives the cross-sectional "dog-bone" shape [1–3], as shown in Fig. 1.

One solution to analyze the vertical rolling is the finite element method (FEM), which can perform complicated calculations under realistic process constraints and various deformation conditions. Huisman and Huetink [4] investigated the influence of roller-radii on the resulting cross section of the slab after a width reduction using a combined Eulerian-Lagrangian three-dimensional finite element method. Using the rigid-plastic FEM, fully theoretical analysis and experimental research for vertical rolling was conducted by Xiong et al. [5]. The research proposed a 3-D model to simulate the vertical rolling, discussed the utilization of the slightly compressible finite element formulation to the numerical analysis of the vertical-horizontal rolling process, and obtained the relationship among section shape after rolling, mechanical parameters and major influence factors [6–9]. However, although the FEM is a very powerful tool for simulation of the rolling process, it is a time-consuming procedure and the accurate setting of the various aspects of the deformation conditions is difficult. At the same time, FEM can only give discrete numerical solutions, not reflect the influence of various mechanical parameters on the stress.

Another approach is analytical solution using kinematically admissible velocity field and minimum energy principle. Yun et al. [10] proposed a new model for the prediction of the dog-bone shape during vertical rolling in roughing mills and examined the results via comparison with predictions from finite element simulation and also with experimental data. However, the explicit mathematical expressions of shape and rolling force are not obtained. The analytical solution can give a continuous analytic expression for the parameters studied, which is the main advantage. And so, analytical methods always have great importance [11].

✉ Jianzhao Cao
caojianzhao@foxmail.com

[1] Information & Control Engineering Faculty, Shenyang Jianzhu University, Shenyang 110168, Liaoning, People's Republic of China

[2] State Key Laboratory of Rolling and Automation, Northeastern University, Shenyang 110819, Liaoning, People's Republic of China

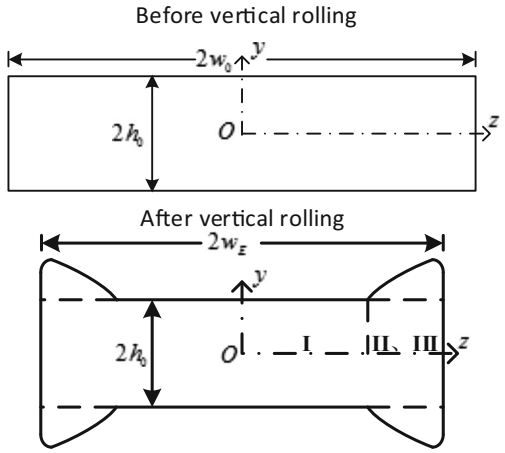

Fig. 1 Cross-sectional shapes of the slab before and after vertical rolling

This paper is to propose an analytical solution based on antisymmetric parabolic dog-bone shape function and an angular bisector yield linear criterion. Using Pavlov principle and integral mean value theorem, the friction power and shear power for vertical rolling are obtained. Then, analytical solution of strip rolling power functional is received. By search method for minimizing the power functional, the rolling force is obtained. Besides, each power including the formula form proposed by this paper is compared with the past one. At the same time, the calculated rolling force and the shape attribute are compared with measured data and other previous publications.

2 Method

2.1 Energy method

Energy method is also called the variational method, which is based on the functional of the Ritz approximation algorithm. The basic analytical steps are described as follows:

(1) Presume the surface shape of the workpiece at some time in a specific forming process, and set a kinematically admissible velocity field including several undetermined parameters under the given boundary conditions.
(2) Build the power functional and minimize it according to the variational principle. The power functional is served as the multivariate function for those undetermined parameters. Then derive its partial derivative of the undetermined parameter and make it to zero, and establish the simultaneous equations containing these undetermined parameters as variables.
(3) Solve the simultaneous equations to obtain the undetermined parameter, and use them to get the kinematically admissible velocity field which is more closely similar to the real one.
(4) Calculate the strain rate field by using the geometric equation, determine the boundary dimension through the displacement of workpiece edge, and determine the mechanical parameters by using the power balance of external and internal forces.

In our opinion, the mathematical method of linearization for the functional integral by transforming the integral terms from strain tensor into inner-product of strain rate vector and summating them to obtain the analytical solution is a new bright spot of the traditional energy method. Meanwhile, building the linear yield criterion corresponded closely to that of Mises in the High-Westergaad space, deriving the linear specific plastic power and using it to replace Mises' nonlinear one, and then making the functional integrable and getting the approximate solution, this is the other highlight which is a new idea for analyzing the material forming from the perspective of a physical method.

2.2 Antisymmetric parabolic dog-bone model

The antisymmetric parabolic model is also called a double parabolic model in ref. [12]. A slab with initial width of $2w_0$ is rolled into a width of $2w_E$ through a pair of vertical rolls of radius R. The coordinate origin is at the midpoint of the entry section and axes x, y, and z are the length, thickness, and width directions, respectively, as shown in Fig. 2. l is the projected length of the contact arc, α is the contact angle, and θ is the bite angle. From the geometry, the contact arc equations for a quarter of deformation zone are as follows:

$$\left.\begin{aligned} w_x &= w_E + R - \sqrt{R^2-(l-x)^2} \\ w_x &= w_\alpha = w_E + R - R\cos\alpha \end{aligned}\right\} \tag{1}$$

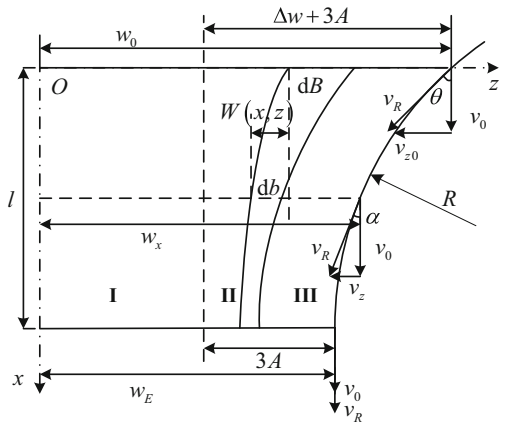

Fig. 2 Deformation zone in vertical rolling

And the first-order derivative is

$$w_x^{'} = -\tan\alpha,\quad \theta = sin^{-1}(l/R) \tag{2}$$

Since w_0/h_0 is relatively large, and $l/\overline{w}$ small, deformation is stopped before extending the center of the work piece; there is a rigid zone in the bite zone, as shown in Fig. 3, which can be divided three zones along the width direction (Yuan-Ming [12]). A is the trisection of zones II and III, and

$$A_x = \frac{w_x-(w_E-3A)}{3} \tag{3}$$

$$3A_x^{'} = w_x^{'} = \tan\alpha, w_x-3A_x = w_E-3A \tag{4}$$

where $A_x = A$ is at the exit of the bite zone and $A_0 = \Delta w/3 + A$ is at the entry.

So, along the thickness direction, dog-bone piecewise function can be expressed as

$$h = \begin{cases} h_{\mathrm{I}} = h_0 & 0 < z < w_E - 3A \\ h_{\mathrm{II}}(x,z) = h_0 + \beta\Delta w_x[z-(w_x-3A_x)]^2 & w_x-3A_x < z < w_x-2A_x \\ h_{\mathrm{III}}(x,z) = h_0 + 2\beta\Delta w_x A_x{}^2 - \beta\Delta w_x[z-(w_x-A_x)]^2 & w_x-2A_x < z < w_x \end{cases} \tag{5}$$

where β is the undetermined parameter. With the assumption of plane strain which occurred in the plastic deformation zone, the area pressed in along the width direction is equal to the area drummed out in zones II and III along the thickness direction (The shaded area is equal as shown in Fig. 3):

$$\Delta w_x h_0 = \int_{w_E-3A}^{w_x-2A_x}(h_{\mathrm{II}}-h_0)\mathrm{d}z + \int_{w_x-2A_x}^{w_x}(h_{\mathrm{III}}-h_0)\mathrm{d}z \tag{6}$$

The peak height of the dog-bone and the edge height of the slab are respectively

$$h_b = h_0 + 2\beta\Delta wA^2,\quad h_r = h_0 + \beta\Delta wA^2 \tag{7}$$

Substituting Eq. (5) into Eq. (6), β is

$$\beta = 3h_0/\left(11A_x^3\right) \tag{8}$$

In Fig. 3, since the half of zone III is antisymmetric with that of zone II, we would rather call it an antisymmetric parabolic model.

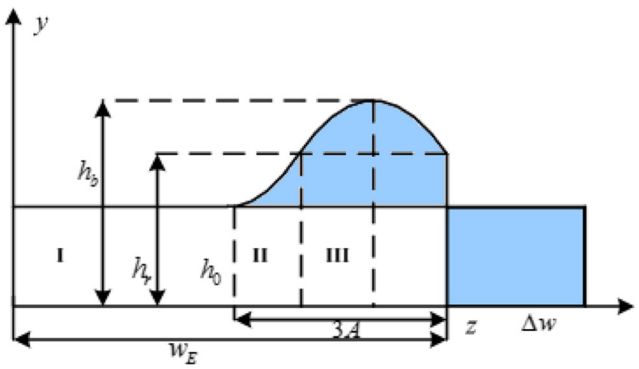

Fig. 3 Antisymmetric parabolic dog-bone shape profile

2.3 Velocity field

As show in Fig. 2, $db-dB$ denotes the change of lateral infinitesimal displacement, $W = W(x,z)$ is the lateral displacement, then

$$\frac{\mathrm{d}W}{\mathrm{d}z} = \frac{\mathrm{d}b-\mathrm{d}B}{\mathrm{d}B} \tag{9}$$

According to the incompressibility condition,

$$v_x = \frac{v_0h_0}{h}\frac{\mathrm{d}B}{\mathrm{d}b} \tag{10}$$

Substituting Eq. (9) into Eq. (10), and taking $\frac{\mathrm{d}W/\mathrm{d}z}{\mathrm{d}W/\mathrm{d}z+1} \approx \frac{\mathrm{d}W}{\mathrm{d}z}$, Eq. (10) becomes:

$$v_x = \frac{v_0h_0}{h}\left(1-\frac{\mathrm{d}W}{\mathrm{d}z}\right) \tag{11}$$

Noticing the property of the stream function $\frac{v_z}{v_x} = \frac{\mathrm{d}W}{\mathrm{d}x}$ yields

$$v_z = v_x\frac{\mathrm{d}W}{\mathrm{d}x} \tag{12}$$

Substituting Eq. (11) into Eq. (12) gives

$$v_z = \frac{v_0h_0}{h}\left(1-\frac{\mathrm{d}W}{\mathrm{d}z}\right)\frac{\mathrm{d}W}{\mathrm{d}x} \tag{13}$$

Because of volume constancy, we have

$$\frac{\partial v_y}{\partial y} + \frac{\partial v_x}{x} = -\frac{\partial v_z}{\partial z} = -\dot{\varepsilon}_z, \dot{\varepsilon}_{\max} = \dot{\varepsilon}_y = \frac{\partial v_y}{\partial y},\quad \dot{\varepsilon}_{\min} = \frac{\partial v_z}{\partial z}. \tag{14}$$

Substituting Eqs. (11) and (13) into Eq. (14), integrating yields

$$\begin{aligned} v_x &= \frac{v_0 h_0}{h}\left(1-\frac{dW}{dz}\right) \\ v_y &= \left\{\left(\frac{\partial W}{\partial z}\text{-}1\right)\left[\frac{\partial}{\partial x}\left(\frac{1}{h}\right)+\frac{\partial}{\partial z}\left(\frac{1}{h}\right)\frac{\partial W}{\partial x}+\frac{1}{h}\frac{\partial^2 W}{\partial x \partial z}\right]+\frac{1}{h}\left[\frac{\partial^2 W}{\partial x \partial z}+\frac{\partial^2 W}{\partial z^2}\cdot\frac{\partial W}{\partial x}\right]\right\} v_0 h_0 y \\ v_z &= \frac{v_0 h_0}{h}\left(1-\frac{dW}{dz}\right)\frac{dW}{dx} \end{aligned} \tag{15}$$

Using the assumption of plane strain and Eq. (15) yields

$$v_x = \frac{v_0 h_0}{h}\left(1-\frac{dW}{dz}\right) = v_0, \quad \frac{dW}{dz} = 1-\frac{h}{h_0} \tag{16}$$

And, lateral displacement W can be integrated:

$$W = \int_0^z \left(1-\frac{h}{h_0}\right) dz \tag{17}$$

Substituting Eq. (5) into Eq. (17), and using the boundary condition, W in zones I, II, and III are

$$\begin{aligned} W_I &= 0, \quad W_{II} = -\frac{\beta \Delta w_x}{3h_0}[z-(w_x-3A_x)]^3, \quad W_{III} \\ &= \frac{\beta \Delta w_x}{3h_0}[z-(w_x-A_x)]^3-\frac{6\Delta w_x}{11A_x}[z-(w_x-A_x)]-\frac{6\Delta w_x}{11} \end{aligned} \tag{18}$$

Substituting Eq. (18) into Eq. (15), velocity and strain rate fields in zone I are

$$v_{xI} = v_0, v_{yI} = v_{zI} = 0; \quad \dot{\varepsilon}_{ij} = 0 \tag{19}$$

Velocity and strain rate fields in zone II are

$$\begin{aligned} v_{xII} &= v_0, v_{yII} \\ &= -\frac{3v_0 w_x'}{11A_x^3}\left(1+\frac{\Delta w_x}{A_x}\right)[z-(w_x-3A_x)]^2 y, v_{zII} \\ &= \frac{v_0 w_x'}{11A_x^3}\left(1+\frac{\Delta w_x}{A_x}\right)[z-(w_x-3A_x)]^3 \end{aligned} \tag{20}$$

$$\dot{\varepsilon}_{xII} = 0, \dot{\varepsilon}_{yII} = -\frac{3v_0 w_x'}{11A_x^3}\left(1+\frac{\Delta w_x}{A_x}\right)[z-(w_x-3A_x)]^2, \quad \dot{\varepsilon}_{zII} = \frac{3v_0 w_x'}{11A_x^3}\left(1+\frac{\Delta w_x}{A_x}\right)[z-(w_x-3A_x)]^2 \tag{21}$$

Velocity and strain rate fields in zone III are

$$\begin{aligned} v_{xIII} &= v_0 \\ v_{yIII} &= \frac{3v_0 y w_x'}{11A_x^3}\left\langle\left\{\left(1+\frac{\Delta w_x}{A_x}\right)[z-(w_x-A_x)]^2+\frac{4\Delta w_x}{3}[z-(w_x-A_x)]\right\}-2A_x^2\left(1+\frac{\Delta w_x}{3A_x}\right)\right\rangle \\ v_{zIII} &= -\frac{v_0 w_x'}{11A_x^3}\left\{\left(1+\frac{\Delta w_x}{A_x}\right)[z-(w_x-A_x)]^3+2\Delta w_x[z-(w_x-A_x)]^2\right\} \\ &+\frac{6v_0 w_x'}{11A_x}\left\{\left(1+\frac{\Delta w_x}{3A_x}\right)[z-(w_x-A_x)]+\frac{2}{3}\Delta w_x+A_x\right\} \end{aligned} \tag{22}$$

$$\begin{aligned} \varepsilon_{xIII} &= 0 \\ \varepsilon_{yIII} &= \frac{3v_0 w_x'}{11A_x^3}\left\langle\left\{\left(1+\frac{\Delta w_x}{A_x}\right)[z-(w_x-A_x)]^2+\frac{4\Delta w_x}{3}[z-(w_x-A_x)]\right\}-2A_x^2\left(1+\frac{\Delta w_x}{3A_x}\right)\right\rangle \\ \varepsilon_{zIII} &= -\frac{3v_0 w_x'}{11A_x^3}\left\langle\left\{\left(1+\frac{\Delta w_x}{A_x}\right)[z-(w_x-A_x)]^2+\frac{4\Delta w_x}{3}[z-(w_x-A_x)]\right\}-2A_x^2\left(1+\frac{\Delta w_x}{3A_x}\right)\right\rangle \end{aligned} \tag{23}$$

From Eqs. (19), (20), (21), (22), and (23), $y=0$, $v_{yII}=0, v_{yIII}=0$; $z=w_x-3A_x, v_{zII}=0$; $z=w_x-2A_x, v_{zIII}=v_{zII}$; $\dot{\varepsilon}_{xII}+\dot{\varepsilon}_{yII}+\dot{\varepsilon}_{zII}=0$; $\dot{\varepsilon}_{xIII}+\dot{\varepsilon}_{yIII}+\dot{\varepsilon}_{zIII}=0$. Clearly, they are kinematically admissible velocity and strain rate fields.

2.4 Angular bisector yield criterion

The unified yield criterion proposed by Yu et al. [13], as we can see in Eq. (24-a), has a unified mechanical model as well

as unified and simple mathematical expression. It includes all independent stress components. It is easily used for analytic solutions because it is a linear yield criterion.

$$\left.\begin{aligned}&\sigma_1-\frac{1}{1+b}(b\sigma_2+\sigma_3)=\sigma_s, when\sigma_2\le\frac{1}{2}(\sigma_1+\sigma_3)\\&\frac{1}{1+b}(\sigma_1+b\sigma_2)-\sigma_3=\sigma_s, when\sigma_2\ge\frac{1}{2}(\sigma_1+\sigma_3)\end{aligned}\right\}\quad(24-\text{a})$$

Angular bisector yield criterion can be deduced from the unified yield criterion when $b=\left(\sqrt{3}-1\right)/2$. It means its yield locus in the π-plane is the bisector of the angle consisting of Tresca's [14] and twin shear stress (TSS) [15] locus, which is also called ID yield criterion because its locus is an inscribed dodecagon of the Mises circle [16]. The comparison of these three linear yield criterion with the Mises yield criterion are shown in Fig. 4. The expressions of the criterion and its specific plastic power are, respectively,

$$\left.\begin{aligned}&\sigma_1-\frac{\sigma_2}{2+\sqrt{3}}-\frac{1+\sqrt{3}}{2+\sqrt{3}}\sigma_3=\sigma_s, \text{when}\sigma_2\le\frac{1}{2}(\sigma_1+\sigma_3)\\&\frac{1+\sqrt{3}}{2+\sqrt{3}}\sigma_1+\frac{\sigma_2}{2+\sqrt{3}}-\sigma_3=\sigma_s, when\sigma_2\ge\frac{1}{2}(\sigma_1+\sigma_3)\end{aligned}\right\},\quad D(\dot{\varepsilon}_{ij})_{ID}=\frac{1}{\sqrt{3}}\sigma_s(\dot{\varepsilon}_{\max}-\dot{\varepsilon}_{\min})\quad(24-\text{b})$$

By contrast, the expressions of specific plastic power for TSS yield criterion using those in ref. [12] are

$$D(\dot{\varepsilon}_{ij})_{TSS}=\frac{2}{3}\sigma_s(\dot{\varepsilon}_{\max}-\dot{\varepsilon}_{\min})\quad(24-\text{c})$$

where σ_s is the yield stress. We can easily find that the formula (24-b) is smaller than (24-c) with the relative error of 13.49 %.

2.5 Internal deformation power

Using angular bisector yield criterion and the strain field, internal deformation power $\dot{W}_i$ in the plastic region can be calculated as follows [17]:

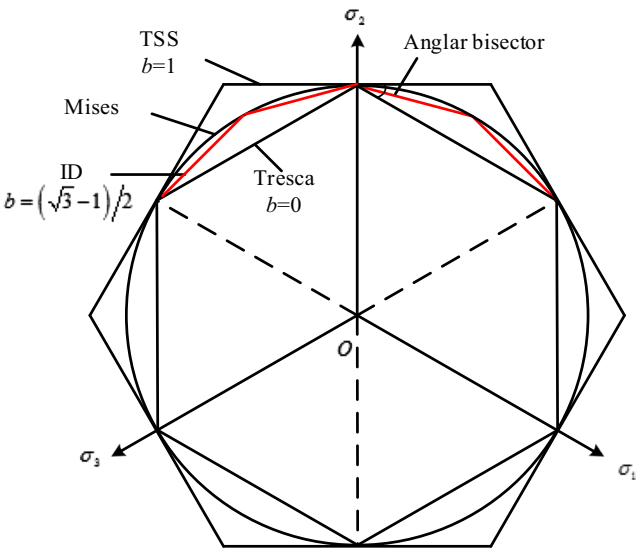

Fig. 4 Yield locus on the π-plane

$$\dot{W}_i=\int_V D(\dot{\varepsilon}_{ij})\mathrm{d}V\quad(25)$$

Substituting Eqs. (21), (23), and (24) into Eq. (25), integrating $\dot{W}_i$ is

$$\begin{aligned}\dot{W}_i&=\dot{W}_{i\mathrm{II}}+\dot{W}_{i\mathrm{III}}\\&=\frac{8\sigma_s v_0 h_0}{121\sqrt{3}}\left[\frac{201\Delta w^2}{5A}-18\Delta w\varepsilon-54A\varepsilon+103\Delta w\right]\end{aligned}\quad(26)$$

where $\varepsilon=\ln[3A/(\Delta w+3A)]$.

Obviously, the internal deformation power deduced in this paper is smaller than that in ref. [12] (Eq. (38)) with the error which is 13 %, and it is more reasonable because of using angular bisector yield criterion which is more approximate to the Mises yield criterion.

2.6 Friction power

The average height of contact surface is taken:

$$\overline{h}_r=(h_r+h_0)/2=h_0+\frac{3h_0\Delta w}{2\times 11A}\quad(27)$$

Assuming the velocity along the length direction and thickness direction are linear distribution, averaging

$$\begin{aligned}v_{y\mathrm{III}}\big|_{x=0}&=\frac{3v_0\,y\tan\theta}{11A_0},\quad v_{y\mathrm{III}}\big|_{x=l}=0,\quad \overline{v}_{y\mathrm{III}}\\&=\frac{3v_0 y\tan\theta}{2\times 11A_0},\quad \overline{v}_{y\mathrm{III}}\big|_{y=0}\\&=0,\ \overline{v}_{y\mathrm{III}}\big|_{y=\overline{h}_r}\frac{3v_0\overline{h}_r\tan\theta}{22A_0},\quad \overline{v}_{y\mathrm{III}}=\frac{3v_0\overline{h}_r\tan\theta}{44A_0}.\end{aligned}$$

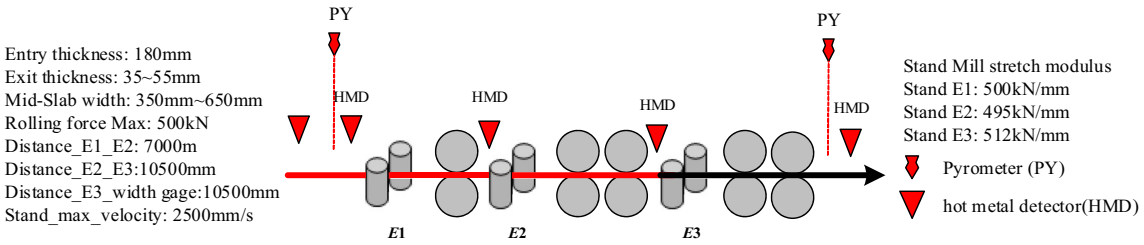

Fig. 5 Schematic diagram and main characteristics of the roughing mill group

With Pavlov projection principle [18], the contact surface and its corresponding tangential velocity discontinuity are projected to the rolling direction, integrating at the projection:

$$\Delta\bar{v}_t = \frac{1}{\theta}\int_0^{\theta}(v_R\cos\alpha - v_0)d\alpha = \frac{\sin\theta}{\theta}v_R - v_0 \tag{28}$$

yields

$$\begin{aligned}\dot{W}_f &= 4\int_{S_f}\tau_f\left|\Delta v_f\right|\mathrm{d}S = 4mk\int_{S_f}\Delta v_f\sqrt{1+w_x'}\,\mathrm{d}y\mathrm{d}x \\ &= 4mk\int_0^{l}\int_0^{\bar{h}_r}\sqrt{\bar{v}_{y\mathrm{III}}^2+\Delta\bar{v}_t^2}\,\mathrm{d}y\mathrm{d}x \\ &= \frac{4m\sigma_s}{\sqrt{3}}\bar{h}_r l\sqrt{\left(\frac{3v_0\bar{h}_r\tan\theta}{44A_0}\right)^2+\left(\frac{\sin\theta}{\theta}v_R-v_0\right)^2}.\end{aligned} \tag{29}$$

It is quite clear that Eq. (29) expresses a simpler formula form than that in ref. [12] (Eq. (51)), and the reason is the application of Pavlov projection principle.

2.7 Shear power

From Eqs. (19), (20), and (22), at the exit of deformation zone, $w_x' = 0$, $v_{y\mathrm{I}} = v_{z\mathrm{I}} = v_{y\mathrm{II}} = v_{z\mathrm{II}} = v_{y\mathrm{III}} = v_{y\mathrm{III}} = 0$, there is no shear power at the exit section but at the entry section. Using mean value theorem of integral:

$$\bar{v}_{y\mathrm{II}} = \frac{\int_0^{h_0}\int_{w_0-3A_0}^{w_0-2A_0}v_{y\mathrm{II}}\mathrm{d}y\mathrm{d}z}{A_0h_0} = \frac{v_0h_0\tan\theta}{22A_0}, \bar{v}_{z\mathrm{II}} = \frac{-v_0\tan\theta}{4\times 11} \tag{30}$$

$$\begin{aligned}\bar{v}_{y\mathrm{III}} &= \frac{\int_0^{h_0}\int_{w_0-3A_0}^{w_0-2A_0}v_{y\mathrm{III}}\mathrm{d}y\mathrm{d}z}{2A_0h_0} = \frac{5v_0h_0\tan\theta}{22A_0}, \bar{v}_{z\mathrm{III}} \\ &= \frac{-6v_0\tan\theta}{11}\end{aligned} \tag{31}$$

Then, the shear power at zone II becomes

$$\begin{aligned}\dot{W}_{s\mathrm{II}} &= 4k\int_{W_0-3A_0}^{W_0-2A_0}\int_0^{h_0}\sqrt{\left(\bar{v}_{y\mathrm{II}}\right)^2+\left(\bar{v}_{z\mathrm{II}}\right)^2}\,dydz \\ &= \frac{2\sigma_s h_0^2 v_0\tan\theta}{11\sqrt{3}}\left[\sqrt{1+\left(\frac{A_0}{2h_0}\right)^2}\right]\end{aligned} \tag{32}$$

And the shear power at zone III is

$$\begin{aligned}\dot{W}_{s\mathrm{III}} &= 4k\int_{w_0-2A_0}^{w_0}\int_0^{h_0}\sqrt{\bar{v}_{y\mathrm{III}}^2+\bar{v}_{z\mathrm{III}}^2}\,dydz \\ &= \frac{20\sigma_s v_0 h_0^2\tan\theta}{11\sqrt{3}}\left[\sqrt{1+\left(\frac{12A_0}{5h_0}\right)^2}\right]\end{aligned} \tag{33}$$

where $A_0 = \Delta w/3 + A$.

It is obvious that the formula of shear power with two terms proposed in this paper is also more simplified than that in ref. [12] (Eq. (45)) which has five more complex terms.

2.8 Total power

The total power J^* can be obtained as follows:

$$J^* = \dot{W}_i + \dot{W}_f + \dot{W}_{s\mathrm{II}} + \dot{W}_{s\mathrm{III}}$$

Table 1 Comparison of calculated rolling forces with the measured ones

Stand no.	v_R (m/s)	t (°C)	$\varepsilon = \ln(h_0/h_1)$	σ_s (MPa)	Calculated force (kN)	Measured force (kN)	Error (%)
$E1$	0.4	1147.4	0.039	38.67	1090.74	1013.94	7.57
$E2$	0.58	1134.45	0.019	31.19	902.17	833.14	8.29
$E3$	1.27	1108.5	0.011	29.64	724.91	686.9	5.53

Table 2 Comparison of calculated powers and rolling forces

	$\dot{W}_i$ (kN·m/s)	$\dot{W}_s$ (kN·m/s)	$\dot{W}_f$ (kN·m/s)	$J^*_{\min}$ (kN·m/s)	Power error (%)	Calculated force (kN)	Force error (%)
Present solution	59.69	45.74	2.35	107.78	−12.01	902.17	−12.02
Past solution	68.92	46.44	7.13	122.49		1025.41	

Summarizing Eqs. (26), (29), (32), and (33), the analytical solution of total deformation power is

$$J^* = \frac{2\sigma_s v_0 h_0}{\sqrt{3}}\left\{\frac{4}{121}\left[\frac{201\Delta w^2}{5A} - 18\Delta w\varepsilon - 54A\varepsilon + 103\Delta w\right] + \frac{h_0\tan\theta}{11}\left[\sqrt{1+\left(\frac{A_0}{2h_0}\right)^2}\right]\right.$$
$$\left. + \frac{10h_0\tan\theta}{11}\left[\sqrt{1+\left(\frac{12A_0}{5h_0}\right)^2}\right] + 2ml\frac{\overline{h}_r}{h_0}\sqrt{\left(\frac{3\overline{h}_r\tan\theta}{44A_0}\right)^2 + \left(\frac{\sin\theta}{\theta}\frac{v_R}{v_0} - 1\right)^2}\right\} \tag{34}$$

where $A_0 = \Delta w/3 + A$. Using a search method, the minimum value of power functional $J^*_{\min}$ and the minimum values of rolling force can be obtained [19], respectively.

$$M_{\min} = \frac{RJ^*_{\min}}{2\nu_R}, F_{\min} = \frac{M_{\min}}{\chi \cdot l} \tag{35}$$

For hot strip rolling, the arm factor χ can be 0.3~0.6 [20], and in this paper, χ is selected as 0.5 under these equipment and process parameters.

3 Results and discussion

3.1 Rolling force and power

In order to verify the validity of the analytical model in this paper, measured data of rolling force in GuoFeng Iron and Steel in HeBei province China are used. The roughing mill group in this factory is composed of three vertical stands and five horizontal stands, and Fig. 5 shows its schematic diagram and main electrical and mechanical characteristics.

Taking the material of Q235 (carbon content 0.14~0.22 %; silicon content <0.3 %; manganese content 0.3–0.65 %; sulfur content <0.05 %; phosphorus content <0.045 %) steel product for instance, the initial width of 150 mm × 380 mm × 6000 mm (thickness × width × length) slab is reduced to 355 mm in the roughing mill. The roll circumferential velocity v_R and temperature t for No.1 to No.3 vertical stands in the roughing mill are shown in Table 1. It should be noticed that the temperatures of $E2$ and $E3$ are determined by temperature self-learning strategy, which can be seen in ref. [21], using the measured temperatures by the thermodetectors at the entrance and exit of the roughing mill. And the rolling forces on-line are monitored by two force transducers,

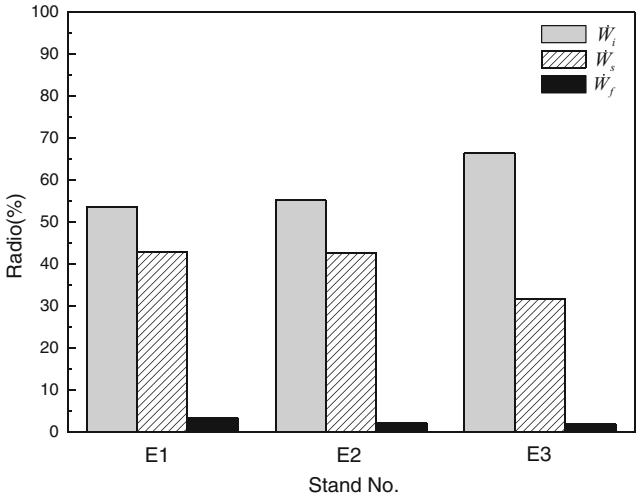

Fig. 6 Ratio of $\dot{W}_i$, $\dot{W}_f$, and $\dot{W}_s$ to $J^*_{\min}$ with a different stand

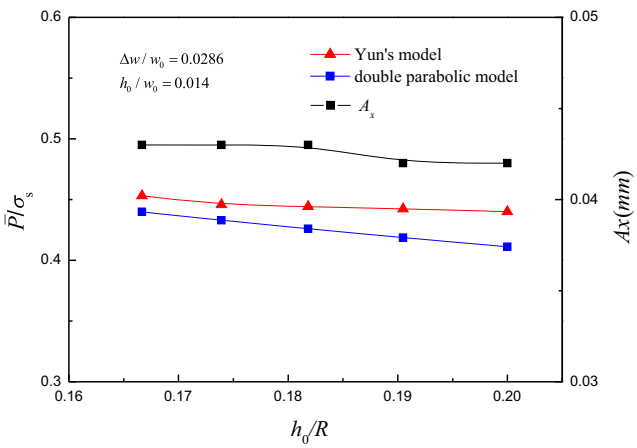

Fig. 7 Effect of h_0/R on $\overline{P}/\sigma_s$ and A_x

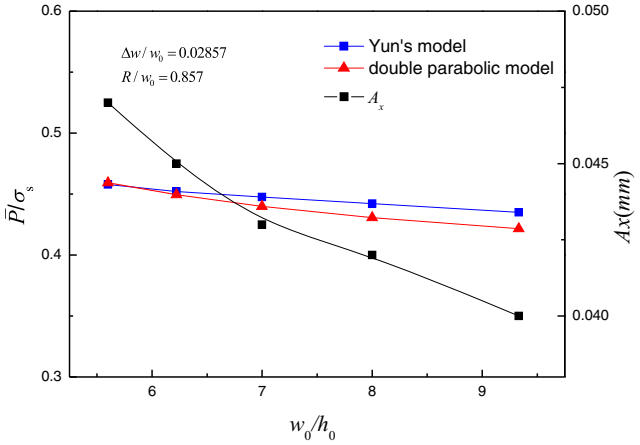

Fig. 8 Effect of w_0/h_0 on $\overline{P}/\sigma_s$ and A_x

located over the bearing blocks of the work roll. The calculated results are compared with the measured ones as shown in Table 1.

The model of deformation resistance for the Q235 steel used in the calculation is determined by Moshitami [22], which can be expressed mathematically as

$$\sigma = \sigma_f f \left(\frac{\dot{\varepsilon}}{10}\right)^m \tag{36}$$

$$\begin{aligned} \sigma_f &= 0.28\exp\left(\frac{5.0}{T} - \frac{0.01}{C+0.05}\right) \quad (T \geq t_d) \\ \sigma_f &= 0.28\exp\left(\frac{5.0}{t_d} - \frac{0.01}{C+0.05}\right) \times g \quad (T \leq t_d) \end{aligned} \tag{37}$$

$$g = 30.0(C+0.90)\left(T - 0.95\frac{C+0.49}{C+0.42}\right)^2 + \frac{C+0.06}{C+0.09} \tag{38}$$

$$f = 1.3\left(\frac{\varepsilon}{0.2}\right)^{0.41-0.07C} - 0.3\left(\frac{\varepsilon}{0.2}\right) \tag{39}$$

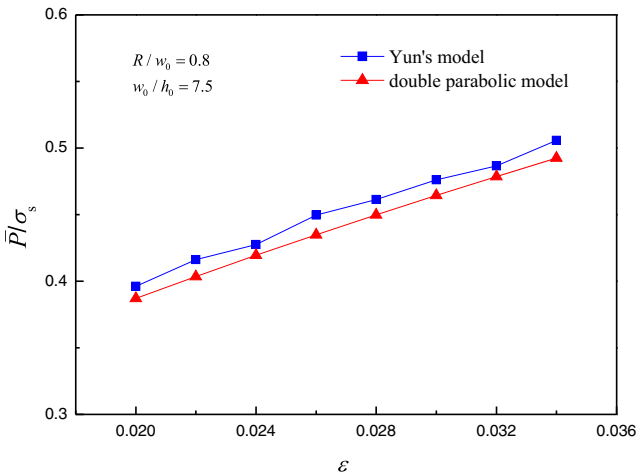

Fig. 9 Effect of ε on $\overline{P}/\sigma_s$

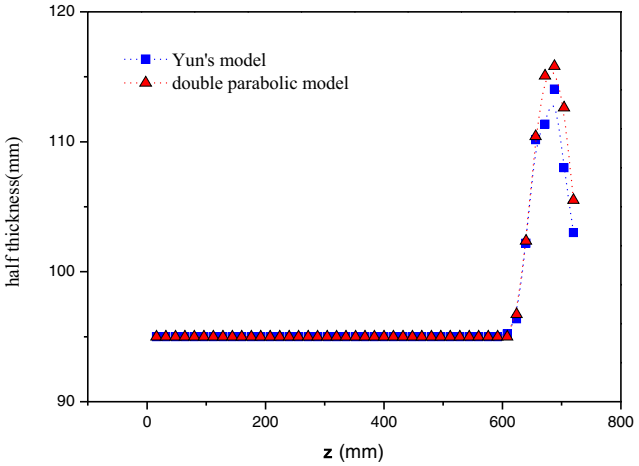

Fig. 10 Comparison of dog-bone shapes

$$\begin{aligned} m &= (0.019C + 0.126)T + (0.075C - 0.05) \quad (T \geq t_d) \\ m &= (0.081C - 0.154)T + (-0.019 + 0.207) + \frac{0.027}{C+0.32} \quad (T \leq t_d) \end{aligned} \tag{40}$$

$$T = \frac{t+273}{1000}, \quad t_d = 0.95\frac{C+0.41}{C+0.32} \tag{41}$$

where t is the deformation temperature (°C), t_d is the critical temperature (°C), and C is the carbon content (%).

Table 2 is the comparison of all calculated powers and rolling force with present solution and past solution in ref. [12] using the practical data of stand $E2$ mentioned above. It shows that each power obtained by the present solution is further lower than that by the past one in ref. [12]. Although the two solutions are all obtained by an upper-bound method, the present solution is more reasonable.

Figure 6 illustrates that the internal plastic deformation power and shear power are the main portion of total power, and friction power is very small, which is different from horizontal rolling (the plastic deformation power and friction power are the main portion) [23, 24]. The reason is that the

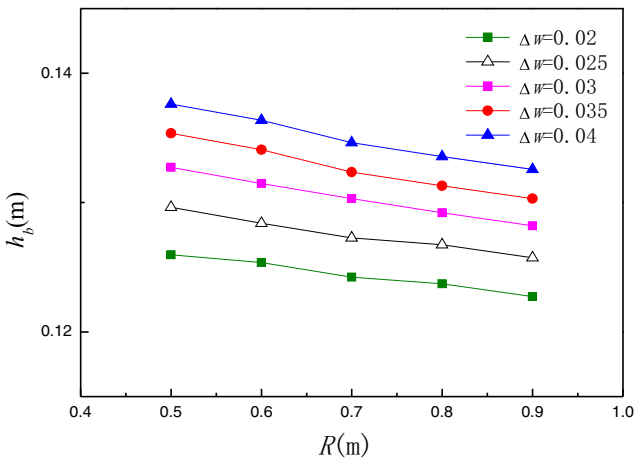

Fig. 11 Effect of R on h_b

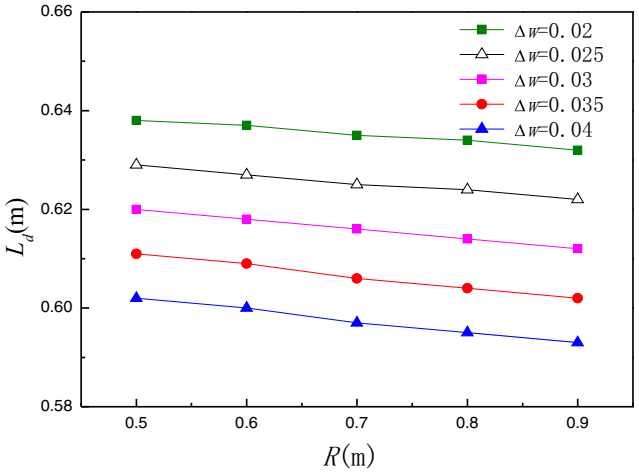

Fig. 12 Effect of R on L_d

length of contact arc l is very small in the vertical rolling with small reduction (3.9, 1.9, and 1.1 %). Moreover, combined with Table 2, the decrease of total power is mainly due to the decrease of the internal deformation power, and the root cause is the use of the ID yield criterion instead of TSS yield criterion.

3.2 Dog-bone shape

Furthermore, for the sake of avoiding impact of deformation resistance, $\overline{P}$ is defined as vertical rolling force per unit thickness as follows:

$$\frac{\overline{P}}{\sigma_s} = \frac{F/\sigma_s}{2h_0} \tag{36}$$

Figure 7 shows the variations of $\overline{P}/\sigma_s$ and A_x with different roll radius. The contact area and length increase while R increases, and then the rolling force and the trisection of the deformation zone (zones II and III) increase, that means the deformation is permeating to the central location of the slab. Figure 8 illustrates that $\overline{P}/\sigma_s$ and A_x decrease with the decrease of h_0. The reason is that the decrease of h_0 makes the decrease in the roll-slab contact arc length; then the internal deformation power decreases, and rigid zone increases.

Figure 9 demonstrates the effect of ε (true strain) on $\overline{P}/\sigma_s$. All the results are in good agreement with Yun's, the maximum error is no more than 10.4 %, and less than the ones in Yun's because of the different integral area. Yun thought that deformation occurred in the entire bite zone, but considering the relatively large width-to-thickness ratio of the slab, there is deformation in the edge of the slab only, so the author believes that the model this paper proposed is more reasonable.

Figure 10 shows that the dog-bone shapes of the two methods, respectively, with the error is no more than 4.2 %. The rolling conditions are $v_R = 1.7$ m/s, $w_0 = 735$ mm, $w_E = 720$ mm, $R = 550$ mm, $h_0 = 95$ mm, and $m = 0.6$, which are taken from Chapter 8 of ref. [10].

Figure 11 shows that the effect of R on h_b. It can be seen that h_b decreases as R increases or Δw decreases. Meanwhile, it also can be seen that the influence of vertical roll diameter for h_b increases with the increment of lateral pressure. So it indicates that a large diameter vertical roll should be adopted to improve rolling efficiency under the condition of large amounts of lateral pressure.

The effect of R on L_d is shown in Fig. 12. It displays that L_d decreases as Δw or R increases. The reason is that increase of Δw makes an increase in the contact arc length, then internal deformation power increases, and rigid zone decreases, and finally causes deformation permeating to the central location of the slab. Besides, it should be pointed out that L_d decreases with the increase of R, because the changes in the width resulted in a more obvious effect than changes in radius.

4 Conclusions

1) Angular bisector linear yield criterion and Pavlov projection principle are first successfully applied in vertical rolling. Using an energy method, simpler analytical solutions of total power and separating rolling force are obtained.
2) The values of calculated rolling force, each power, and the dog-bone shape parameters are compared with measured ones and previous models, and the results show good agreement.
3) In vertical rolling with small reduction, the internal plastic deformation power and shear power are the main portion of total power, which is different from horizontal rolling.
4) The present solution gives lower total power than that in ref. [12] with a relative error of 12 % because the TSS specific plastic power is higher than that of angular bisector yield criterion by 13.49 %.

Acknowledgments The authors wish to acknowledge the financial support received from the National Natural Science Foundation of China (Grant No. 51074052, 50734002).

References

1. Xiong S, Rodrigues JMC, Martins PAF (2003) Three-dimensional modelling of the vertical–horizontal rolling process. Finite Elem Anal Des 39(11):1023–1037
2. Du XZ, Yang Q, Lu C, Wang AL, Kiet TA (2010) Optimization of short stroke control preset for automatic width control of hot rolling mill. J Iron Steel Res Int 17(6):16–20
3. Ginzburg VB (1989) Steel-rolling technology: theory and practice. Marcel Dekker, Inc., New York

4. Huisman HJ, Huetink J (1985) A combined Eulerian-Lagrangian three-dimensional finite-element analysis of edge-rolling. J Mech Working Technol 3(11):333–353
5. Xiong S, Liu X, Wang G, Zhang Q (1997) Simulation of slab edging by the 3-D rigid-plastic FEM. J Mater Process Technol 69(1-3):37–44
6. Xiong S, Liu X, Wang G, Martins PAF, Jiao S, Yuan J (2001) Three-dimensional thermo-mechanical finite element simulation of the vertical–horizontal rolling process. J Mater Process Technol 110(1):89–97
7. Xiong S, Liu X, Wang G, Zhang Q (2000) A three-dimensional finite element simulation of the vertical–horizontal rolling process in the width reduction of slab. J Mater Process Technol 101(1-3): 146–151
8. Xiong S, Zheng G, Xianghua L, Wang G (2002) Analysis of the non-steady state vertical–horizontal rolling process in roughing trains by the three-dimensional finite element method. J Mater Process Technol 120(1-3):53–61
9. Xiong S, Liu X, Wang G, Zhang W (1997) Simulation of vertical horizontal rolling process during width reduction by full three dimensional rigid plastic finite element method. J Mater Eng Perform 6(6):757–76
10. Yun D, Lee D, Kim J, Hwang S (2012) A new model for the prediction of the dog-bone shape in steel mills. ISIJ Int 52(6): 1109–1117
11. Luis CJ, Le´on J, Luri R (2005) Comparison between finite element method and analytical methods for studying wire drawing processes. J Mater Process Technol 164:1218–1225
12. Liu Y-M, Zhang D-H, Zhao D-W, Sun J (2015) Analysis of vertical rolling using double parabolic model and stream function velocity field. Int J Adv Manuf Technol. In press. doi: 10.1007/s00170-015-7393-7
13. Yu M, He L, Liu C (1992) Generalized twin-shear stress yield criterion and its generalization. Chin Sci Bull 37(24):2085–2089
14. Tresca H (1983) On the flow of solid bodies subjected to high pressures. Int J Mech Sci 25:71–74
15. Yu M (1983) Twin shear stress yield criterion. Int J Mech Sci 25(1): 71–74
16. Zhao D (2012) The principle and application of integrating linearization for deformation power. Metallurgical Industry Press, Beijing **(in Chinese)**
17. Zhao D, Zhang S, Li C, Song H, Wang G (2012) Rolling with simplified stream function velocity and strain rate vector inner product. J Iron Steel Res 19(3):20–24
18. Павлов И. М (1950) Теория прокаткн. Металлургиэцат
19. Zhang SH, Zhao DW, Gao CR (2012) The calculation of roll torque and roll separating force for broadside rolling by stream function method. Int J Mech Sci 57(1):74–78
20. Klarin K, Mouton JP, Lundberg SE (1993) Application of computerized slip-linefield analysis for the calculation of the lever-arm coefficient in hot-rolling mills. J Mater Process Technol 36(4): 427–446
21. Li H-j, Shi L-j, Xu J-z, Wang G-d (2009) Temperature model of hot strip finishing mills in tandem and its self-learning strategy. J Northeastern Univ (Natural science) 30(3):369–372
22. Moshitami (1969). Empirical formula of deformation resistance of carbon steel. Plastic Processing 10(97): 103-107
23. Zhang D-h, Cao J-z, Xu J-j, Peng W, Zhao D-w (2014) Simplified weighted velocity field for prediction of hot strip rolling force by taking into account flattening of rolls. J Iron Steel Res Int 21(7): 637–634
24. Zhang D-H, Liu Y-M, Sun J, Zhao D-W (2015) A novel analytical approach to predict rolling force in hot strip finish rolling based on cosine velocity field and equal area criterion. Int J Adv Manuf Technol. In press. doi: 10.1007/s00170-015-7692-z